On the measurement of the dielectric properties of anisotropic biological tissues using electrical impedance

H. Kwon[1], S.B. Rutkove[1], B. Sanchez[1]

[1]Department of Neurology, Beth Israel Deaconess Medical Center, Harvard Medical School, Boston, MA 02215-5491, USA
Contact: hkwon1@bidmc.harvard.edu

Introduction

Measuring the dielectric properties conductivity and relative permittivity of biological tissues is important to understanding how electromagnetic fields interact with biological systems. Moreover, these two physical quantities are essential to apply new imaging modalities for medical purposes [1, 2]. When applying impedance methods to biological tissues, electrical current may flow in a certain direction which is determined by the directional dependence (also known as anisotropy) of the conductivity and relative permittivity. For example, in muscle tissue, the anisotropy is determined by the orientation of the muscle fibers [3,4] and in vivo study in rat muscle reported a 10 times difference between longitudinal (current flow along the muscle fibers) and transverse (current flow perpendicular to the muscle fibers) conductivity values [5].

Currently available impedance approaches for measuring in situ the anisotropy dielectric properties are based on the following assumptions:

(i) The anisotropic material is purely conductive and so the relative permittivity is zero.
(ii) The four-electrode probe is aligned in the direction determined by the known anisotropy.

However, (i) tissues have non-zero relative permittivity, and (ii), positioning the four-electrode probe in longitudinal and transverse directions with accuracy may be difficult depending on the a priori knowledge of the anisotropy. Here, new electrical impedance methods are presented for measuring in situ the dielectric properties of anisotropic tissues [6]. The new methods allow us to estimate the anisotropy in both the conductivity and relative permittivity and do not require to align the four-electrode probe in any prespecified direction.

Methods

We extend the major result of Rush's work [7]. To make the analysis feasible, we consider the same anisotropy ratio α^2 in the conductivity σ (S m^{-1}) and relative permittivity ε_r (dimensionless) properties in longitudinal (L) and transverse (T) directions, i.e. $\alpha^2 := \sigma_{\mathrm{T}}/\sigma_{\mathrm{L}} = \varepsilon_{r,\mathrm{T}}/\varepsilon_{r,\mathrm{L}}$. In this case, the electric potential V (V) can be written as follows

$$V = \frac{\kappa_\alpha I}{K\,|r_\alpha|}, \tag{1}$$

where I (A) is the total current; $K \in \{2\pi, 4\pi\}$ is the constant factor (dimensionless) for semi-infinite $\mathbb{R}^3_-$ and infinite $\mathbb{R}^3$ domains, respectively; $\kappa_\alpha := \sqrt{\kappa_{\mathrm{L}}\,\kappa_{\mathrm{T}}}$ (Ω m) is the geometric mean impedivity (Ω m) computed using the longitudinal (L) and transverse (T) impedivity $\kappa_{\{\mathrm{L,T}\}}$, defined as

$$\kappa_{\{\mathrm{L,T}\}} := \rho_{\{\mathrm{L,T}\}} + j\tau_{\{\mathrm{L,T}\}} \tag{2}$$

where the real part $\rho = (\sigma + (\omega\varepsilon_0\varepsilon_r)^2/\sigma)^{-1}$ and imaginary part $\tau = -j(\sigma^2/\omega\varepsilon_0\varepsilon_r + \omega\varepsilon_0\varepsilon_r)^{-1}$ of the impedivity are the resistivity and reactivity (Ω m), respectively; ε_0 is the vacuum permittivity (F m^{-1}); ω is the angular frequency (rad s^{-1}); and $j^2 = -1$ is the imaginary unit (dimensionless). The apparent impedivity κ_{a} measured with a four-electrode probe placed on the surface of the semi-infinite domain (see schematic in fig. 1) follows,

$$\kappa_{\mathrm{a}}(\theta) = \rho_{\mathrm{a}}(\theta) + j\tau_{\mathrm{a}}(\theta) = \frac{\kappa_{\mathrm{L}}}{l_{\alpha,\theta}\,\alpha} \tag{3}$$

where $l_{\alpha,\theta} := \sqrt{\cos^2\theta + \alpha^2\sin^2\theta}$ (dimensionless), and $\theta \in [0,\pi]$ is the angle (rad) between the transverse direction determined by the tissues' anisotropy (x-axis) and the direction determined by the four-electrode probe.

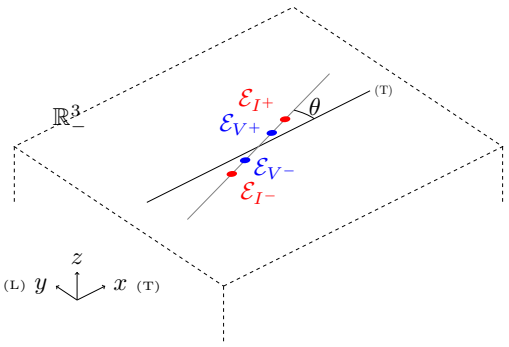

Figure 1: Schematic illustrating of four-electrode probe placed on the surface of the semi-infinite domain $\mathbb{R}^3_-$. Current electrodes $\mathscr{E}_{I^{+,-}}$ (red), voltage electrodes $\mathscr{E}_{V^{+,-}}$ (blue). $\theta \in [0,\pi]$ is the the angle measured with the probe (direction shown in gray color) with respect to the transverse (T) direction determined by the tissues' anisotropy (x-axis). Longitudinal (L) direction y-axis.

Next we present four methods for estimating both the longitudinal and transverse resistivity $\widehat{\rho}_{\{\mathrm{L,T}\}}$ and reactivity $\widehat{\tau}_{\{\mathrm{L,T}\}}$, and the anisotropy ratio $\widehat{\alpha}^2$. The new methods use (3) noisy apparent resistivity $\rho_{\mathrm{a}}^{[m]}(\theta)$ and apparent reactivity $\tau_{\mathrm{a}}^{[m]}(\theta)$ data. The methods are identified as C1 to C4.

Method C1: The apparent resistivity and apparent reactivity are measured in two angles $\rho_{\mathrm{a}}^{[m]}(\theta_1)$, $\tau_{\mathrm{a}}^{[m]}(\theta_1)$, $\rho_{\mathrm{a}}^{[m]}(\theta_2)$, $\tau_{\mathrm{a}}^{[m]}(\theta_2)$ with $\theta_1 \perp \theta_2$ and $\theta_{\{1,2\}} \in \mathbb{R}$.

Assumption 1 The longitudinal and transverse directions defined by the resistivity and reactivity are known so that the measuring angle $\theta = \phi_{\mathrm{T}}$ when $\theta = 0$.

Assumption 2 The measured angles $\theta_{\{1,2\}}$ are the longitudinal and transverse directions defined by the resistivity and reactivity, i.e. $\theta_1 = \phi_{\mathrm{L}}$ and $\theta_2 = \phi_{\mathrm{T}}$.

The anisotropy ratio $\widehat{\alpha}^2$, and the longitudinal and transverse resistivity $\widehat{\rho}_{\{\mathrm{L,T}\}}$ and reactivity $\widehat{\tau}_{\{\mathrm{L,T}\}}$ can be estimated as follows

$$\left\{\begin{array}{lcll} \widehat{\alpha}^2 & := & \widehat{\rho}_{\mathrm{a}}{}^2(\phi_{\mathrm{T}})/\widehat{\rho}_{\mathrm{a}}{}^2(\phi_{\mathrm{L}}) & \text{or} \quad \widehat{\tau}_{\mathrm{a}}{}^2(\phi_{\mathrm{T}})/\widehat{\tau}_{\mathrm{a}}{}^2(\phi_{\mathrm{L}}) \\ \widehat{\rho}_{\mathrm{L}} & := & \widehat{\alpha}^2\widehat{\rho}_{\mathrm{a}}(\phi_{\mathrm{L}}) & \text{and} \quad \widehat{\rho}_{\mathrm{T}} := \widehat{\rho}_{\mathrm{a}}(\phi_{\mathrm{T}})/\widehat{\alpha} \\ \widehat{\tau}_{\mathrm{L}} & := & \widehat{\alpha}^2\widehat{\tau}_{\mathrm{a}}(\phi_{\mathrm{L}}) & \text{and} \quad \widehat{\tau}_{\mathrm{T}} := \widehat{\tau}_{\mathrm{a}}(\phi_{\mathrm{T}})/\widehat{\alpha}. \end{array}\right. \tag{4}$$

Note that one can choose estimating anisotropy ratio $\widehat{\alpha}^2$ using $\widehat{\rho}_{\mathrm{a}}$ or $\widehat{\tau}_{\mathrm{a}}$. The choice of one or the other should be based on the noise level of both the apparent resistivity and apparent reactivity.

Method C2: The apparent resistivity and apparent reactivity are measured two angles $\rho_{\mathrm{a}}^{[m]}(\theta_1)$, $\rho_{\mathrm{a}}^{[m]}(\theta_2)$, $\tau_{\mathrm{a}}^{[m]}(\theta_1)$, $\tau_{\mathrm{a}}^{[m]}(\theta_2)$ with $\theta_{\{1,2\}} \in \mathbb{R}$.

Assumption 1 Same as Assumption 1 in Method C1.

Assumption 2 The measuring angles $\theta_{\{1,2\}}$ satisfy $\tan^2\theta_1 \neq \tan^2\theta_2$.

The anisotropy ratio $\widehat{\alpha}^2$, and the longitudinal and transverse resistivity $\widehat{\rho}_{\{\mathrm{L,T}\}}$ and reactivity $\widehat{\tau}_{\{\mathrm{L,T}\}}$ can be estimated as follows

$$\left\{\begin{array}{lcl} \widehat{\alpha}^2 & := & 1 + \frac{\widehat{\rho}_{\mathrm{a}}{}^2(\theta_1) - \widehat{\rho}_{\mathrm{a}}{}^2(\theta_2)}{\widehat{\rho}_{\mathrm{a}}{}^2(\theta_2)\sin^2\theta_2 - \widehat{\rho}_{\mathrm{a}}{}^2(\theta_1)\sin^2\theta_1} \\ & \text{or} & 1 + \frac{\widehat{\tau}_{\mathrm{a}}{}^2(\theta_1) - \widehat{\tau}_{\mathrm{a}}{}^2(\theta_2)}{\widehat{\tau}_{\mathrm{a}}{}^2(\theta_2)\sin^2\theta_2 - \widehat{\tau}_{\mathrm{a}}{}^2(\theta_1)\sin^2\theta_1} \\ \widehat{\rho}_{\mathrm{L}} & := & \frac{1}{2}\sum_{i=1}^{2}\widehat{\rho}_{\mathrm{a}}(\theta_i) l_{\widehat{\alpha},\theta_i}\widehat{\alpha} \\ \widehat{\rho}_{\mathrm{T}} & := & \frac{1}{2}\sum_{i=1}^{2}\widehat{\rho}_{\mathrm{a}}(\theta_i) l_{\widehat{\alpha},\theta_i}/\widehat{\alpha} \\ \widehat{\tau}_{\mathrm{L}} & := & \frac{1}{2}\sum_{i=1}^{2}\widehat{\tau}_{\mathrm{a}}(\theta_i) l_{\widehat{\alpha},\theta_i}\widehat{\alpha} \\ \widehat{\tau}_{\mathrm{T}} & := & \frac{1}{2}\sum_{i=1}^{2}\widehat{\tau}_{\mathrm{a}}(\theta_i) l_{\widehat{\alpha},\theta_i}/\widehat{\alpha}. \end{array}\right. \tag{5}$$

The same observation as method C1 applies here when estimating $\widehat{\alpha}^2$.

Method C3: The apparent resistivity and apparent reactivity are measured in $D \geq 2$ angles $\rho_{\mathrm{a}}^{[m]}(\theta_d)$, $\tau_{\mathrm{a}}^{[m]}(\theta_d)$ with $\theta_d \in [0,\pi)$.

Case 1: $D = 2$.

Assumption 1 Same as Assumption 1 in Method C1.

Assumption 2 Same as Assumption 2 in Method C2.

Case 2: $D \geq 3$.

Assumption 1 Same as Assumption 1 in Method C1.

Method C3 is computed using the matrices $\mathbf{M}$ and $\mathbf{N}$ with sizes $D \times 2$ and a vector $\mathbf{b}$ with size $D \times 1$, defined by

$$\mathbf{M} := \begin{bmatrix} \widehat{\rho}_{\mathrm{a}}{}^2(\theta_1)\cos^2\theta_1 & \widehat{\rho}_{\mathrm{a}}{}^2(\theta_1)\sin^2\theta_1 \\ \widehat{\rho}_{\mathrm{a}}{}^2(\theta_2)\cos^2\theta_2 & \widehat{\rho}_{\mathrm{a}}{}^2(\theta_2)\sin^2\theta_2 \\ \vdots & \vdots \\ \widehat{\rho}_{\mathrm{a}}{}^2(\theta_D)\cos^2\theta_D & \widehat{\rho}_{\mathrm{a}}{}^2(\theta_D)\sin^2\theta_D \end{bmatrix},$$

$$\mathbf{N} := \begin{bmatrix} \widehat{\tau}_{\mathrm{a}}{}^2(\theta_1)\cos^2\theta_1 & \widehat{\tau}_{\mathrm{a}}{}^2(\theta_1)\sin^2\theta_1 \\ \widehat{\tau}_{\mathrm{a}}{}^2(\theta_2)\cos^2\theta_2 & \widehat{\tau}_{\mathrm{a}}{}^2(\theta_2)\sin^2\theta_2 \\ \vdots & \vdots \\ \widehat{\tau}_{\mathrm{a}}{}^2(\theta_D)\cos^2\theta_D & \widehat{\tau}_{\mathrm{a}}{}^2(\theta_D)\sin^2\theta_D \end{bmatrix}$$

and $\mathbf{b} := [1\ 1\ \cdots\ 1]^\top$ so that $\widehat{\mathbf{v}} = [\widehat{v}_1\ \widehat{v}_2]^\top$ and $\widehat{\mathbf{u}} = [\widehat{u}_1\ \widehat{u}_2]^\top$ can be obtained as $\widehat{\mathbf{v}} = (\mathbf{M}^\top\mathbf{M})^{-1}\mathbf{M}^\top\mathbf{b}$ and $\widehat{\mathbf{u}} = (\mathbf{N}^\top\mathbf{N})^{-1}\mathbf{N}^\top\mathbf{b}$, respectively. The anisotropy ratio $\widehat{\alpha}^2$, longitudinal and transverse resistivity $\widehat{\rho}_{\{\mathrm{L,T}\}}$ and reactivity $\widehat{\tau}_{\{\mathrm{L,T}\}}$ can be estimated as follows

$$\left\{\begin{array}{lcll} \widehat{\alpha}^2 & := & \widehat{v}_2/\widehat{v}_1 & \text{or} \quad \widehat{u}_2/\widehat{u}_1 \\ \widehat{\rho}_{\mathrm{L}} & := & \sqrt{\widehat{v}_2}/\widehat{v}_1 & \text{and} \quad \widehat{\rho}_{\mathrm{T}} := 1/\sqrt{\widehat{v}_2} \\ \widehat{\tau}_{\mathrm{L}} & := & -\sqrt{\widehat{u}_2}/\widehat{u}_1 & \text{and} \quad \widehat{\tau}_{\mathrm{T}} := -1/\sqrt{\widehat{u}_2}. \end{array}\right. \tag{6}$$

The same observation as method C1 applies here when estimating $\widehat{\alpha}^2$.

Simulation verification methods C1, C2 and C3

A comparison of methods C1 to C3 at 10 kHz is shown in fig. 2. We use transverse resistivity $\rho_{\mathrm{T}} = 2.93\ \Omega$ m and transverse relative permittivity $\varepsilon_{r,\mathrm{T}} = 2.59 \cdot 10^4$ (dimensionless) from skeletal muscle at 10 kHz [8]. The anisotropy ratio is $\alpha^2 = 0.5$, and so the longitudinal resistivity is $\rho_{\mathrm{L}} = 1.47\ \Omega$ m. We generated a vector of $M = 10$ apparent resistivity and reactivity measurements containing Gaussian additive noise of zero mean with a signal-to-noise ratio (SNR) of 20 dB (MATLAB, The Mathworks, Inc., Natick, MA).

Method C4: The apparent resistivity and apparent reactivity are measured in $D \geq 3$ angles $\rho_{\mathrm{a}}^{[m]}(\theta_d)$, $\tau_{\mathrm{a}}^{[m]}(\theta_d)$ with $\theta_d \in [0,\pi)$.

Assumption 1 None

All previous methods assume $\theta = \phi_{\mathrm{T}}$ when $\theta = 0$ and consequently $\theta = \phi_{\mathrm{L}}$ when $\theta = \pi/2$, see the x and y axes in fig. 2. Therefore, methods C1 to C3 will give inaccurate results if: (1), the experimental positioning of the electrodes' array with respect the anisotropy in the impedivity of the tissue is inaccurate, or (2), the true anisotropy on the impedivity is unknown.

The error caused by a misalignment of ξ is studied below with the anisotropy ratio of muscle $\alpha^2 = 0.1$ [5]. When a misalignment of $\xi = 1^\circ$ placing the four-electrode probe with respect to the longitudinal and transverse anisotropy directions, the relative error in the estimation of the anisotropy ratio $\widehat{\alpha}^2$ is 0.3%. As the misalignment increases, the error increases rapidly. These relative error will increase the smaller α^2. For example, the relative error is 8% for $\xi = 5^\circ$, 31% for $\xi = 10^\circ$, and 71% for $\xi = 15^\circ$.

Method C4 below does not need to align the four-electrode probe in any direction. To do that, the complexity of the apparent impedivity model includes the uncertainty in positioning the four-electrode probe:

$$\kappa_{\mathrm{a}}(\theta,\xi) = \frac{\kappa_{\mathrm{L}}}{l_{\alpha,\theta,\xi}\,\alpha}, \tag{7}$$

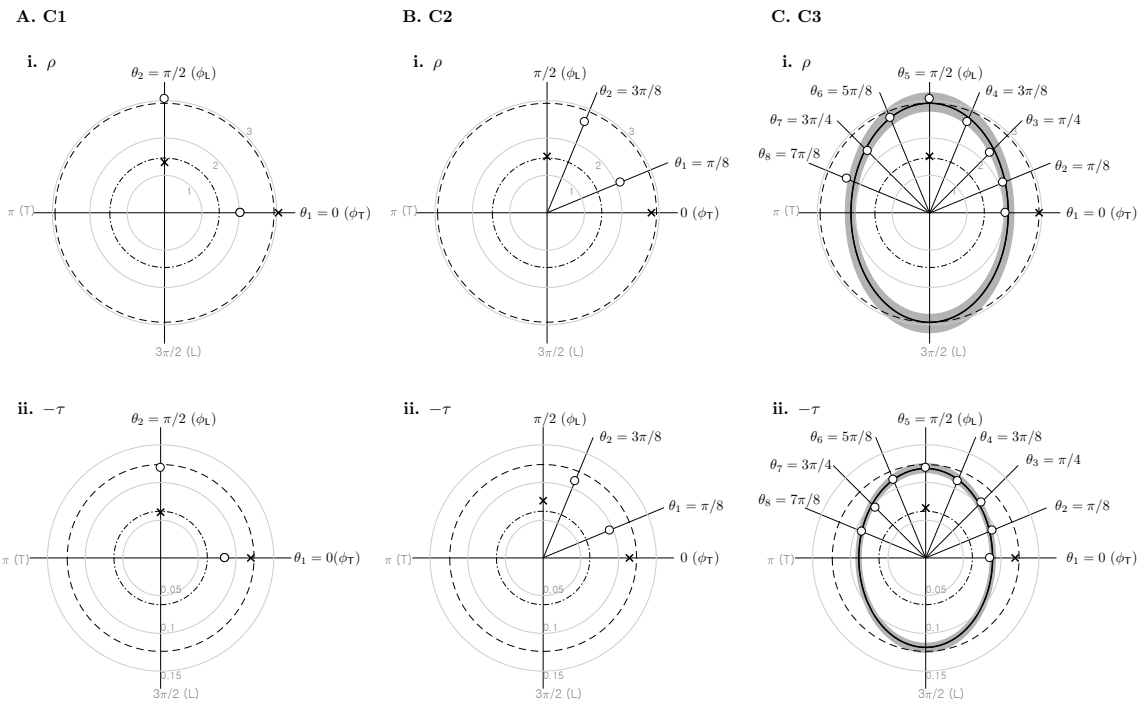

Figure 2: Representative polar plots using method C1 (A), method C2 (B), and method C3 (C). The longitudinal (L) and transverse (T) resistivity $\widehat{\rho}_{\{\mathrm{L,T}\}}$ (i) and reactivity $\widehat{\tau}_{\{\mathrm{L,T}\}}$ (ii) are estimated (in crosses) from $M = 10$ averaged apparent resistivity $\widehat{\rho}_{\mathrm{a}}(\theta)$ and apparent reactivity $\widehat{\tau}_{\mathrm{a}}(\theta)$ measurements (in circles). Method C1: $\widehat{\rho}_{\mathrm{L}} = 1.35\ \Omega$ m, $\widehat{\rho}_{\mathrm{T}} = 3.05\ \Omega$ m, $\widehat{\tau}_{\mathrm{L}} = -0.06\ \Omega$ m, $\widehat{\tau}_{\mathrm{T}} = -0.12\ \Omega$ m; Method C2: $\widehat{\rho}_{\mathrm{L}} = 1.51\ \Omega$ m, $\widehat{\rho}_{\mathrm{T}} = 2.79\ \Omega$ m, $\widehat{\tau}_{\mathrm{L}} = -0.08\ \Omega$ m, $\widehat{\tau}_{\mathrm{T}} = -0.11\ \Omega$ m; Method C3: $\widehat{\rho}_{\mathrm{L}} = 1.51\ \Omega$ m, $\widehat{\rho}_{\mathrm{T}} = 2.93\ \Omega$ m, $\widehat{\tau}_{\mathrm{L}} = -0.07\ \Omega$ m, $\widehat{\tau}_{\mathrm{T}} = -0.12\ \Omega$ m. The true longitudinal and transverse resistivities (i) and reactivities (ii) are shown for comparison purposes in dash-dot and dotted circumferences, $\rho_{\mathrm{L}} = 1.46\ \Omega$ m, $\rho_{\mathrm{T}} = 2.93\ \Omega$ m, $\tau_{\mathrm{L}} = -0.06\ \Omega$ m and $\tau_{\mathrm{T}} = -0.12\ \Omega$ m, respectively. In method C3, the solid black line is the adjusted apparent resistivity (i) and reactivity (ii) and the shaded area represents its 99% confidence interval. As a convention, $-\tau$ is shown. The units are Ω m.

where $l_{\alpha,\theta,\xi} := \sqrt{\cos^2(\theta-\xi)+\alpha^2\sin^2(\theta-\xi)}$ (dimensionless) and ξ (rad) is defined as the angle between the probe axis and the true anisotropy in the longitudinal and transverse impedivity of the tissue. Method C4 is computed using the matrices $\mathbf{M}$ and $\mathbf{N}$ with sizes $D \times 3$ and a vector $\mathbf{b}$ with size $D \times 1$, defined as

$$\mathbf{M} := \begin{bmatrix} \widehat{\rho}_{\mathrm{a}}^{\,2}(\theta_1)\cos^2\theta_1 & \widehat{\rho}_{\mathrm{a}}^{\,2}(\theta_1)\sin^2\theta_1 & \widehat{\rho}_{\mathrm{a}}^{\,2}(\theta_1)\cos\theta_1\sin\theta_1 \\ \widehat{\rho}_{\mathrm{a}}^{\,2}(\theta_2)\cos^2\theta_2 & \widehat{\rho}_{\mathrm{a}}^{\,2}(\theta_2)\sin^2\theta_2 & \widehat{\rho}_{\mathrm{a}}^{\,2}(\theta_2)\cos\theta_2\sin\theta_2 \\ \vdots & \vdots & \vdots \\ \widehat{\rho}_{\mathrm{a}}^{\,2}(\theta_D)\cos^2\theta_D & \widehat{\rho}_{\mathrm{a}}^{\,2}(\theta_D)\sin^2\theta_D & \widehat{\rho}_{\mathrm{a}}^{\,2}(\theta_D)\cos\theta_D\sin\theta_D \end{bmatrix}, \quad (8)$$

$$\mathbf{N} := \begin{bmatrix} \widehat{\tau}_{\mathrm{a}}^{\,2}(\theta_1)\cos^2\theta_1 & \widehat{\tau}_{\mathrm{a}}^{\,2}(\theta_1)\sin^2\theta_1 & \widehat{\tau}_{\mathrm{a}}^{\,2}(\theta_1)\cos\theta_1\sin\theta_1 \\ \widehat{\tau}_{\mathrm{a}}^{\,2}(\theta_2)\cos^2\theta_2 & \widehat{\tau}_{\mathrm{a}}^{\,2}(\theta_2)\sin^2\theta_2 & \widehat{\tau}_{\mathrm{a}}^{\,2}(\theta_2)\cos\theta_2\sin\theta_2 \\ \vdots & \vdots & \vdots \\ \widehat{\tau}_{\mathrm{a}}^{\,2}(\theta_D)\cos^2\theta_D & \widehat{\tau}_{\mathrm{a}}^{\,2}(\theta_D)\sin^2\theta_D & \widehat{\tau}_{\mathrm{a}}^{\,2}(\theta_D)\cos\theta_D\sin\theta_D \end{bmatrix} \quad (9)$$

and $\mathbf{b} := [1\ 1\ \cdots\ 1]^\top$ so that $\widehat{\mathbf{\Pi}} = \left[\widehat{\Pi}_1\ \widehat{\Pi}_2\ \widehat{\Pi}_3\right]^\top$ and $\widehat{\mathbf{\Sigma}} = \left[\widehat{\Sigma}_1\ \widehat{\Sigma}_2\ \widehat{\Sigma}_3\right]^\top$ can be calculated as $\widehat{\mathbf{\Pi}} = (\mathbf{M}^\top\mathbf{M})^{-1}\mathbf{M}^\top\mathbf{b}$ and $\widehat{\mathbf{\Sigma}} = (\mathbf{N}^\top\mathbf{N})^{-1}\mathbf{N}^\top\mathbf{b}$, respectively. Next, we can define the following quantities

$$\widehat{\nu}_1 := \left((\widehat{\Pi}_1+\widehat{\Pi}_2)+\sqrt{(\widehat{\Pi}_1-\widehat{\Pi}_2)^2+\widehat{\Pi}_3^2}\right)\Big/2, \quad (10)$$

$$\widehat{\nu}_2 := \left((\widehat{\Pi}_1+\widehat{\Pi}_2)-\sqrt{(\widehat{\Pi}_1-\widehat{\Pi}_2)^2+\widehat{\Pi}_3^2}\right)\Big/2, \quad (11)$$

$$\widehat{u}_1 := \left((\widehat{\Sigma}_1+\widehat{\Sigma}_2)+\sqrt{(\widehat{\Sigma}_1-\widehat{\Sigma}_2)^2+\widehat{\Sigma}_3^2}\right)\Big/2, \text{ and} \quad (12)$$

$$\widehat{u}_2 := \left((\widehat{\Sigma}_1+\widehat{\Sigma}_2)-\sqrt{(\widehat{\Sigma}_1-\widehat{\Sigma}_2)^2+\widehat{\Sigma}_3^2}\right)\Big/2. \quad (13)$$

The anisotropy ratio $\widehat{\alpha}^2$, longitudinal and transverse resistivity $\widehat{\rho}_{\{\mathrm{L,T}\}}$ and reactivity $\widehat{\tau}_{\{\mathrm{L,T}\}}$ can be estimated as follows

$$\begin{cases} \widehat{\alpha}^2 & := & \widehat{\nu}_2/\widehat{\nu}_1 & \text{or} & \widehat{u}_2/\widehat{u}_1 \\ \widehat{\rho}_{\mathrm{L}} & := & \sqrt{\widehat{\nu}_2}/\widehat{\nu}_1 & \text{and} & \widehat{\rho}_{\mathrm{T}} := 1/\sqrt{\widehat{\nu}_2} \\ \widehat{\tau}_{\mathrm{L}} & := & -\sqrt{\widehat{u}_2}/\widehat{u}_1 & \text{and} & \widehat{\tau}_{\mathrm{T}} := -1/\sqrt{\widehat{u}_2}. \end{cases} \quad (14)$$

Experimental results

Impedance measuring devices and electrode matrix

We measured in situ impedance of muscle using SFB7 (Impedimed Inc., Brisbane, Australia) between 10 kHz and 1 MHz (203 frequencies) with a custom made electrode matrix. The electrode matrix was designed on a printed circuit board (PCB) for in situ measurements. In PCB, 32 spring-loaded pin type electrodes (Interconnect Devices Inc., ref. S-100-T-6.7-G) were equipped so that the pin electrodes

can contact with the non-regular surface of the sample tissue. There are two concentric circles in the electrode matrix with radii 15 and 20 mm giving a 8 different angles $\theta_{\{1,\cdots,8\}}$ in $[0,\ \pi]$.

In situ impedance measurements

We performed in situ experiments at the Animal Research Facility of Beth Israel Deaconess Medical Center in Boston, MA. Animals were measured postmortem, so this study did not require Institutional Animal Care and Use Committee approval. We measured healthy skeletal muscle tissues in situ from freshly killed sheep ($n = 3$) at room temperature (25 °C) within 30 minutes after the animals were euthanized. We used a scalpel to expose large and regular segments of medius gluteus muscles to reflect back the overlying skin and subcutaneous fat. We gently press the electrode matrix to ensure the electrical contact of all the electrodes with the muscle.

Data analysis

The apparent impedance values (Ω) measured in situ were normalized to impedivity values (Ω m) by calibration measurements in reference saline solution. We plot the real and imaginary parts of the complex permittivity $\varepsilon := \varepsilon' - j\varepsilon'' = \varepsilon_r - j\sigma/\omega\varepsilon_0$ (dimensionless) against the frequency to facilitate the comparison with other studies available in the literature (fig. 3). Note that from the definition κ, we have

$$\varepsilon' = -\frac{\tau}{\omega\varepsilon_0(\rho^2+\tau^2)} \quad \text{and} \quad \varepsilon'' = -\frac{\rho\varepsilon_0}{\tau}. \qquad (15)$$

Below, we detail the data-driven approach to implement method C4:

1. Measure apparent impedivity κ_a using (3).
2. Compute $\mathbf{M}$ and $\mathbf{N}$ using (8,9).
3. Compute $\widehat{\mathbf{\Pi}} = (\mathbf{M}^\top\mathbf{M})^{-1}\mathbf{M}^\top\mathbf{b}$ and $\widehat{\mathbf{\Sigma}} = (\mathbf{N}^\top\mathbf{N})^{-1}\mathbf{N}^\top\mathbf{b}$ where $\mathbf{b} = [1\ 1\ \cdots\ 1]^\top$.
4. Compute $\widehat{v}_1$, $\widehat{v}_2$, $\widehat{u}_1$, $\widehat{u}_2$ using (10-13).
5. Obtain $\widehat{\alpha}^2$, $\widehat{\rho}_L$, $\widehat{\rho}_T$, $\widehat{\tau}_L$, $\widehat{\tau}_T$ using (14).
6. Obtain complex permittivity ε' and ε'' using (15).

Discussion

Here, we provided electrical impedance methods for estimating the conductivity and relative permittivity properties of anisotropic biological tissues using electrical impedance technique. In particular, method C4 does not require to align four-electrode probe in any preferred direction and can be applied to measure anisotropy changes in diseased muscle, e.g. to detect the loss of anisotropy in dystrophic muscle [9]. Future work will focus on extending the existing methods when the anisotropy of the conductivity and relative permittivity are different, i.e. $\alpha^2 \neq \beta^2$.

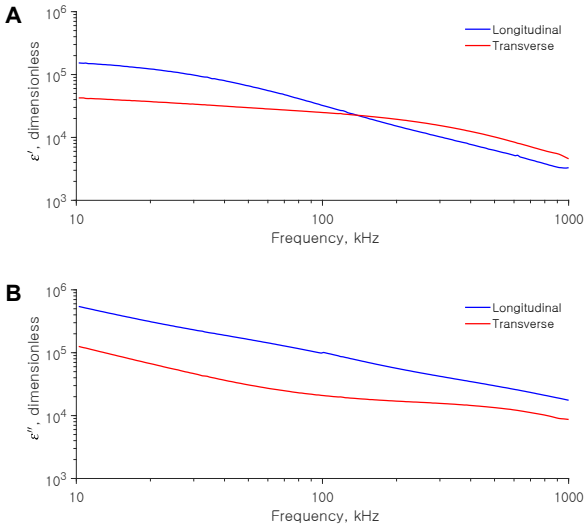

Figure 3: Estimated real ε' (A) and imaginary ε'' (B) parts of the complex permittivity ε of muscle measured ex vivo in longitudinal (blue) and transverse (red) directions.

References

[1] D S Holder. *Electrical Impedance Tomography: Methods, History and Applications.* Institute of Physics, 2004.

[2] Jin Keun Seo and Eung Je Woo. Magnetic Resonance Electrical Impedance Tomography (MREIT). *SIAM Rev.*, 53(1):40–68, jan 2011.

[3] P Fatt. An analysis of the transverse electrical impedance of striated muscle. *Proc. R. Soc. London. Ser. B, Biol. Sci.*, 159:606–51, mar 1964.

[4] B. R. Epstein and K. R. Foster. Anisotropy in the dielectric properties of skeletal muscle. *Med. Biol. Eng. Comput.*, 21(1):51–55, jan 1983.

[5] F. L. H. Gielen, W. Wallinga-de Jonge, and K. L. Boon. Electrical conductivity of skeletal muscle tissue: Experimental results from different muscles in vivo. *Med. Biol. Eng. Comput.*, 22(6):569–577, nov 1984.

[6] H Kwon, J A Nagy, R Taylor, S B Rutkove, and B Sanchez. New electrical impedance methods for the in situ measurement of the complex permittivity of anisotropic biological tissues. *Physics in Medicine & Biology*, 62(22):8616, 2017.

[7] S Rush. Methods of measuring the resistivities of anisotropic conducting media in situ. *J. Res. Natl. Bur. Stand. Sect. C Eng. Instrum.*, 66C(3):217, 1962.

[8] D Andreuccetti, R Fossi, and C Petrucci. An Internet resource for the calculation of the dielectric properties of body tissues in the frequency range 10 Hz - 100 GHz, 1997.

[9] Seward B. Rutkove, Jim S. Wu, Craig Zaidman, Kush Kapur, Sung Yim, Amy Pasternak, Lavanya Madabusi, Heather Szelag, Tim Harrington, Jia Li, Adam Pacheck, and Basil T. Darras. Loss of electrical anisotropy is an unrecognized feature of dystrophic muscle that may serve as a convenient index of disease status. *Clin. Neurophysiol.*, 127(12):3546–3551, dec 2016.